A framework for separating natural and anthropogenic contributions to evapotranspiration of human-managed land covers in watersheds based on machine learning

Hongwei Zeng [a,b], Abdelrazek Elnashar [a,b,c], Bingfang Wu [a,b,*], Miao Zhang [a], Weiwei Zhu [a], Fuyou Tian [a], Zonghan Ma [a]

[a] State Key Laboratory of Remote Sensing Science, Aerospace Information Research Institute, Chinese Academy of Sciences, Beijing 100101, China
[b] College of Resources and Environment, University of Chinese Academy of Sciences, Beijing 100049, China
[c] Department of Natural Resources, Faculty of African Postgraduate Studies, Cairo University, Giza 12613, Egypt

HIGHLIGHTS

- A framework to separate ET_n and ET_h of human-managed land cover types
- ET_n and ET_h were quantified for four human-managed land covers in three basins.
- Human activities that occur in drier basins tend to increase water depletion more significantly.

GRAPHICAL ABSTRACT
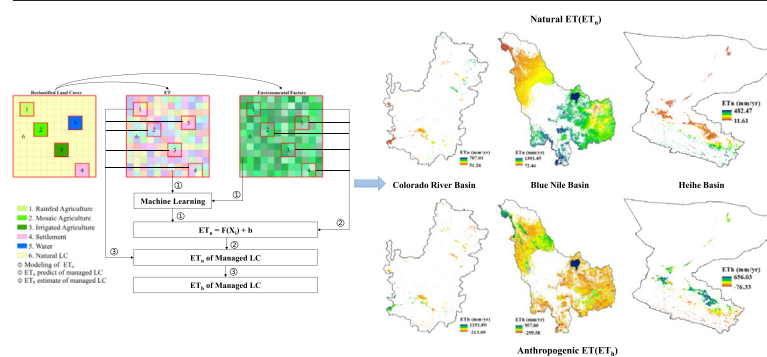
ARTICLE INFO

ABSTRACT

Actual EvapoTranspiration (ET) represents the water consumption in watersheds; distinguishing between natural and anthropogenic contributions to ET is essential for water conservation and ecological sustainability. This study proposed a framework to separate the contribution of natural and anthropogenic factors to ET of human-managed land cover types using the Random Forest Regressor (RFR). The steps include: (1) classify land cover into natural and human-managed land covers and then divide ET, meteorological, topographical, and geographical data into two parts corresponding to natural and human-managed land cover types; (2) construct a natural ET (ET_n) prediction model using natural land cover types of ET, and the corresponding meteorological, topographical and geographical factors; (3) the constructed ET_n prediction model is used to predict the ET_n of human-managed land cover types using the corresponding meteorological, topographical and geographical data as inputs, and (4) derive the anthropogenic ET (ET_h) by subtracting the natural ET from the total ET (ET_t) for human-managed land cover types. Take 2017 as an example, ET_n and ET_h for rainfed agriculture, mosaic agriculture, irrigated agriculture, and settlement in Colorado, Blue Nile, and Heihe Basin were separated by the proposed framework, with R^2 and NSE of predicted ET_n above 0.95 and RB within 1% for all three basins. In the semi-arid Colorado River Basin and arid Heihe Basin, human activities on human-managed land cover types tended to increase ET higher than humid Blue Nile Basin. The anthropogenic contribution to total water consumption is approaching 53.68%, 66.47%, and 6.14% for the four human-managed land cover types in Colorado River Basin, Heihe Bain and Blue Nile Basin, respectively. The

---

* Corresponding author at: State Key Laboratory of Remote Sensing Science, Aerospace Information Research Institute, Chinese Academy of Sciences, Beijing 100101, China.
E-mail address: wubf@aircas.ac.cn (B. Wu).

framework provides strong support for the disturbance of water resources by different anthropogenic activities at the basin scale and the accurate estimation of the impact of human activities on ET to help achieve water-related sustainable development goals.

1. Introduction

Actual EvapoTranspiration (ET) is a key variable linking ecosystem function, carbon, climate change, agricultural management, and water resources (Fisher et al., 2017). As the largest water consumption, ET account for 2/3 of global terrestrial precipitation (Oki and Kanae, 2006). In the past 15 years, Global terrestrial ET has shown an increasing trend (Pascolini-Campbell et al., 2021; Zhang et al., 2019). Regional runoff management and the expansion of irrigation increased freshwater consumption of 3563 ± 979 km^3 yr^{-1} from 1901–1954 to 1955–2008 (Jaramillo and Destouni, 2015). Of all human activities, agriculture is the largest user and consumer of water resources, with irrigation accounting for 70% of total global water use for human activities (Döll and Siebert, 2002; Siebert et al., 2010). The total annual global water consumption for irrigation is estimated at 1250 km^3 (Hoff et al., 2010), accounting for 87% of total water consumption for human activities (Döll and Siebert, 2002). Human activities are considered a major contributor to the increased ET and ecosystem damage. A study by Zou et al. (2017) found that human agricultural activities and climate change increased ET per unit area at rates of 53.86–60.93% and 28.01%–35.68% in the agricultural areas of the Heihe Basin (Zou et al., 2017). The "Grain to Green" revegetation program on the Loess Plateau in China has led to an increase of ET, causing regional water consumption to be approaching the limits of sustainable water resources (Feng et al., 2016). Therefore, controlling and reducing ET from human activities is key to achieving water-related sustainable developments goals (SDG 6) of the United Nations (Ho et al., 2020; Taing et al., 2021).

In order to quantify the total water consumption, several evapotranspiration models have been developed over the past decades, which have produced several regional and global evapotranspiration remote sensing products (FAO and IHE Delft, 2020; Senay et al., 2013; Zhang et al., 2019). For example, the operational Simplified Surface Energy Balance model (SSEBop) has produced decadal, monthly, and annual ET products at 1000 m spatial resolution since 2003 (Senay et al., 2013). The Penman-Monteith-Leuning model (PML) has generated global ET products at 500 m spatial resolution from 2002 to 2017 (Zhang et al., 2019). The current study found that trends in different ET datasets showed significant differences in magnitude and direction (Kim et al., 2021). For this reason, different fusion methods have been proposed to synthesize ET (Elnashar et al., 2021b; Wang et al., 2021). For example, Elnashar et al. (2021b) used a data fusion approach to generate a global monthly evapotranspiration dataset with a spatial resolution of 1000 m from 1982 to 2019. These ET data can provide data support for assessing a basin scale's total water consumption.

However, it is not enough to know the total water consumption in the basin, but the role and contribution of human activities in ET need to be clarified to support water consumption regulation. It is extremely challenging to separate the contribution of natural and human activities to ET and quantitatively assess the impact of different human activities on ET. Due to the diversity and complexity of human activities compounded with climate change (Mao et al., 2015), it is difficult to calculate the contribution of human activities to ET directly. Therefore, current studies generally use indirect methods to estimate the contribution of human activities to ET. These approaches first calculate ET due to natural factors (herein defined as ET$_n$) and then calculate the difference between total ET and ET$_n$ as the anthropogenic contribution to ET (ET$_h$).

ET$_n$ can be described as ET$_n$ = $\omega \ast$ P, where P is precipitation, and ω is a coefficient between 0 and 1, which varies with climate, terrain, and soil conditions (Bastiaanssen et al., 2014). ω is often set as a constant value to estimate ET$_n$ at the basin scale, such as the Nile River Basin (Bastiaanssen

et al., 2014), Incomati Basin (van Eekelen et al., 2015), and Lake Ebinur (Zeng et al., 2019). These approaches rely heavily on expert experience and are subject to uncertainty due to the significant heterogeneity of the watershed. In order to reduce uncertainties, some equations based on aridity index have been proposed to estimate the ω, such as the Budyko curve (Budyko, 1974), but these empirical equations ignore the influence of topography, soil, and geographical factors on ω, resulting in widely varying ω values obtained with different empirical equations.

The development of remote sensing technology provides new solutions for the estimation of ET$_n$. The coupled Gravity Recovery and Climate Experiment (GRACE) data and land surface hydrological models approach are currently the main methods for separating anthropogenic contributions and natural factors. The method uses GRACE data to estimate total ET and a surface hydrological model to estimate ET without anthropogenic disturbance; the difference of them is the anthropogenic contribution to the total ET (Castle et al., 2016; Pan et al., 2017). Using this method, Castle estimated that human activities contributed 12% of the total ET of the Colorado River Basin (Castle et al., 2016), and Pan determined that human activities caused a 12% increase in ET in the Haihe Basin (Pan et al., 2017). However, there are obvious shortcomings in this method. One is the coarse spatial resolution of GRACE data, which is only suitable for watersheds larger than 200,000 km^2 (Rodell and Famiglietti, 1999); second is that the regional gravity change signal reflected by GRACE is not only the change of water storage but also includes the gravity change caused by energy and mineral extraction and the entry and exit of goods in the region. For example, in the North China Plain, the gravity anomaly caused by coal transportation reaches 1.9 mm yr^{-1} (Tang et al., 2013). Third, the method can only calculate the impact of human activities on the total ET of the basin but cannot quantify the amount of change in basin ET caused by different human activities, such as irrigated and rainfed croplands.

The scenario assumption is another way to estimate ET$_n$, taking the separation of natural and anthropogenic water consumption in cropland as an example, which treats the ET generated from uncropped land as the ET generated by natural factors, and then uses spatial interpolation to estimate the natural ET from cropland in the entire study area. The difference between total ET and natural ET is the ET generated by anthropogenic activities in cropland (Wu et al., 2018). However, this approach is greatly limited by the number of uncropped land pixels and spatial distribution, resulting in large errors in separating natural and anthropogenic ET.

Land cover can be regarded as a bridge to distinguish between natural and anthropogenic properties of ET. A shift in land cover type due to human activities can alter soil water content and the water cycle, increase (weaken) the ET capacity of vegetation, and change the magnitude of regional ET. The distinction between natural and anthropogenic properties of ET has also been developed based on land cover properties (van Eekelen et al., 2015). For example, Karimi et al. (2013) classified land use into "conserved land use", "utilized land use", "modulated land use", and "artificial land use" based on the characteristics of land use, and proposed the water accounting (WA+) framework. Bastiaanssen et al. used the WA+ framework to account for water production and consumption in the Nile Basin (Bastiaanssen et al., 2014). However, this framework also does not address the separation of natural and anthropogenic ET in artificial land cover.

The mechanisms of regional water depletion by climate change and human activities are complex. Climate change exacerbates regional water scarcity (Gosling and Arnell, 2016), particularly as 15% of the global population will face severe water scarcity when global temperatures rise by 2 °C (Schewe et al., 2014). The effects of irrigation on ET from agricultural land are complex (Ozdogan et al., 2010); agricultural land under irrigation changes soil water content, water availability and distribution, soil

temperature, surface fluxes, and ET (Leng et al., 2014). Under the influence of climate change, increasing irrigation water demand could lead to local and regional irrigation water crises (Leng et al., 2015). Therefore, it is important to specify the amount of water consumed on agricultural land due to cultivation and management to achieve sustainable agricultural water management.

Machine learning (ML) and cloud computing have flourished in recent years. Machine learning and deep learning are widely used in landcover classification, change detection, and image feature extraction but are limited in water resources studies (Shen, 2018). However, it has already shown a powerful mining capability in hydrological studies. For instance, ML was used to estimate production flow coefficients (Yan et al., 2019), streamflow modeling (McNamara et al., 2021), and spatiotemporal downscaling of precipitation (Elnashar et al., 2020). In this study, we employed the ML to separate between natural and anthropogenic properties of ET. To the best of our knowledge, this is the first time ML has been used to separate ET. Furthermore, ML requires powerful computational resources. With the development of earth observation technologies, particularly the emergence of remote sensing big data cloud platforms that provide powerful computing, data processing, and analytical capabilities, such as Google Earth Engine (GEE) (Gorelick et al., 2017). GEE has been successfully used in some environmental studies to retrieve and process Earth observation data (e.g., Elnashar et al., 2021c; Zeng et al., 2020). New opportunities are available to quantify the impact of large regional scales, complex climate change, and human activities on ET.

This study intends to clarify the contributions of natural factors and human activities to ET of human-managed land cover types from a data-driven perspective using the powerful data mining capabilities and cloud computing capacity. The objectives of this study include (1) constructing a framework to separate natural and anthropogenic contributions to ET of managing land covers in watersheds at the pixel level; (2) quantifying the role and contribution of human activities in ET of human-managed land cover types in the Colorado River Basin, Blue Nile Basin, and Heihe Basin.

2. Data and method

2.1. Study area

The Colorado River Basin, Blue Nile Basin, and Heihe Basin are selected as the study area (Fig. 1 and Table 1). Colorado River Basin includes parts of seven U.S. states and Mexico. The Colorado River Basin covers approximately 630,000 km^2 and is dominated by a semi-arid climate with an average annual precipitation of 400 mm yr^{-1}. 79% of the flow originates from snowmelt, and 15% of the area contributes 85% of the streamflow (Christensen and Lettenmaier, 2007). The Blue Nile Basin is located in Eastern Africa and is shared by Ethiopia and Sudan, with an approximate drainage area of 312,000 km^2. The Inter-Tropical Convergence Zone dominates the upper Blue Nile Basin climate, and the semi-arid climate controls the downstream in Sudan (Taye et al., 2015). The annual average precipitation and ET of the Blue Nile Basin estimated by remote sensing data were about 978 mm yr^{-1} and 737 mm yr^{-1}, respectively (Bastiaanssen et al., 2014). The Blue Nile Basin contributes approximately 60% of the total river flow of the Nile River, reaching Aswan High Dam in Egypt (Senay et al., 2014). The Heihe Basin is the second-longest inland basin in China, covers 143,200 km^2, and has a high altitude, complex terrain, various ecosystems, and harsh climate (Che et al., 2019). Frozen soil water, glacial or snow meltwater, and precipitation contributes 11%, 23%, and 66% of streamflow of the Heihe Basin, and its glaciated areas shrank by 30.0% due to
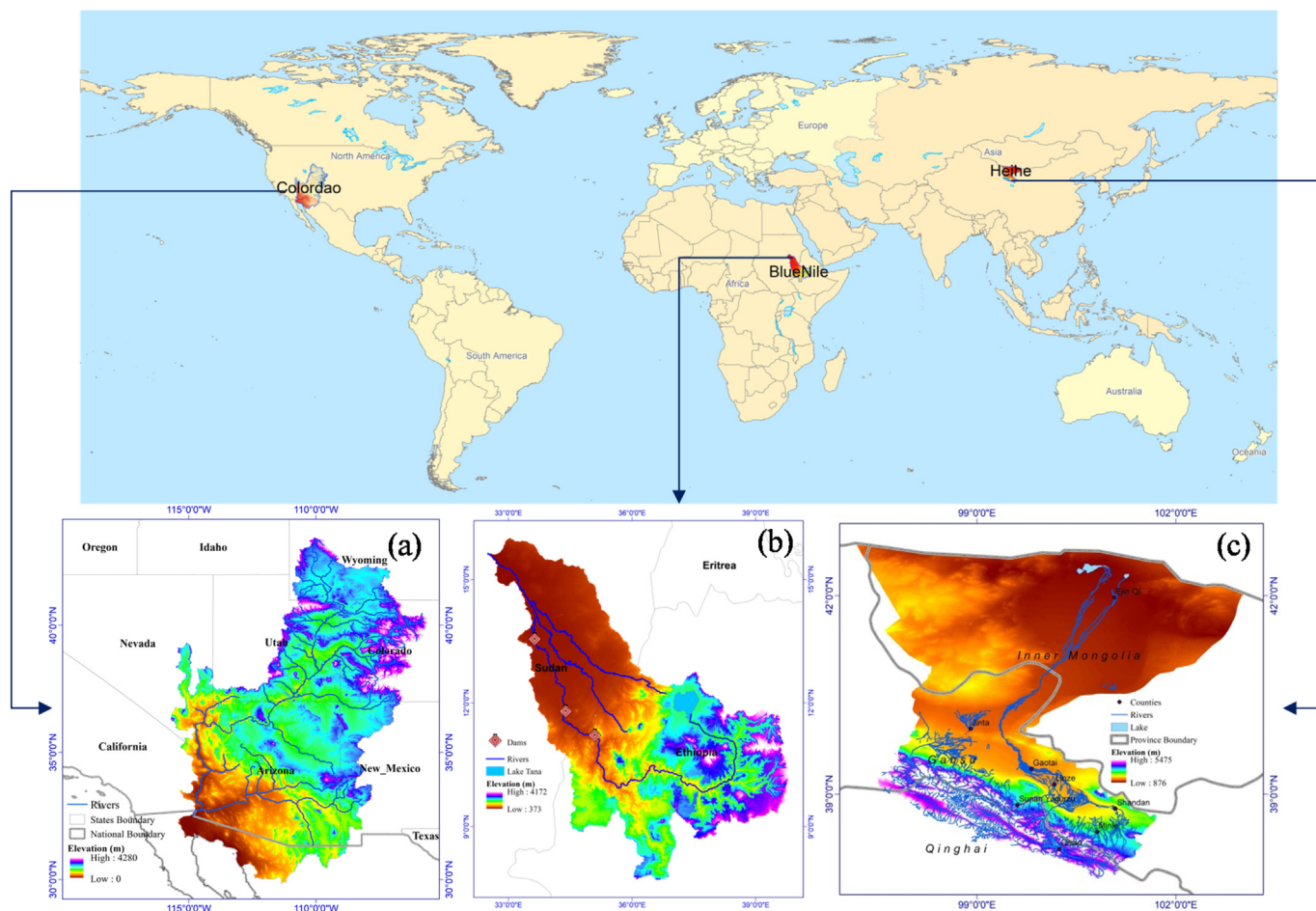

Fig. 1. The geographical location of the Colorado River Basin (a), Blue Nile Basin (b), and Heihe Basin (c).

Table 1

Features summary of Colorado River Basin, Blue Nile Basin, and Heihe Basin.

Basin name	Area (km^2)	Climate	Contributor of runoff (%)	Water issues
Colorado River	630,000	Semi-arid	Snowmelt (79)	Allocation of water rights
Blue Nile	312,000	Humid (Ethiopia), semi-arid (Sudan)	Precipitation (100)	Soil erosion, water conflict between upper and downstream
Heihe	143,200	Arid	Precipitation (66)	Ecological damage caused by over-consumption of irrigation water for agriculture
			Snowmelt (23)	
			Frozen soil water (11)	

the warming trend (Chen et al., 2019b). The runoff flow of the Heihe River from the Qilian Mountains is the only water source for industry and agriculture in the arid middle and downstream areas (Kang et al., 1999).

2.2. Data

The free and open data sources from GEE, including the ET, meteorological, topographic, and geographic data, are used to promote the public usability of this work.

2.2.1. Evapotranspiration

Several satellite-based ET models have been developed to quantify the total water consumption of watersheds over the past decades, while these satellite-based ET products are subject to biases in their algorithms, parameters, and inputs (Wang and Dickinson, 2012; Weerasinghe et al., 2020; Xu et al., 2019). These uncertainties can be reduced by synthesizing multiple satellite ET products under different conditions using different strategies (Badgley et al., 2015; Mueller et al., 2013; Vinukollu et al., 2011; Wang et al., 2021). For this purpose, the synthesized ET product at a 1 km spatial resolution for 2017 was used in this study (Elnashar et al., 2021b). This dataset was generated from the simple average of the Penman-Monteith-Leuning (PML) (Zhang et al., 2019) and the operational Simplified Surface Energy Balance (SSEBop) (Senay et al., 2013) remote sensing ET products. It can be retrieved from the following link: https://doi.org/10.7910/DVN/ZGOUED.

2.2.2. Environmental factors

Meteorological, topographic, geographic location data are used as input variables to build the ET separation model in the RFR algorithm. To avoid the interference of the difference of data magnitude on the regression model construction, this study standardized all features by their mean and standard deviation to eliminate the effects of different scales (Elnashar et al., 2020).

2.2.2.1. Meteorological data.
In this study, precipitation (P), downward long-wave radiation flux (LWdown), downward shortwave radiation flux (DWdown), air temperature (Tair), wind speed (Wind), Pressure (Psurf), and specific humidity (Qair) are used as meteorological factors to build ET contribution separation model. Precipitation data were generated from the Climate Hazards Group InfraRed Precipitation with Station data (CHIRPS) (Funk et al., 2015). CHIRPS is a daily $0.05° \times 0.05°$ (≈ 5 km) grid cell quasi-global rainfall dataset from 1981. It creates a gridded rainfall product by incorporating the remotely sensed precipitation with in-situ station data. LWdown, downward, DWdown, Tair, Wind, and Psurf with a spatial resolution of $0.25°$ (≈ 25 km) were generated from the Global Land Data Assimilation System (GLDAS-2.1) (Rodell et al., 2004). GLDAS-2.1 was preferred given it combined satellite and ground-based observations and generated optimal fields of land surface states and fluxes through advanced surface modeling and data assimilation techniques. Furthermore, it was widely used in similar previous studies (e.g., Ning et al., 2014; Zhang et al., 2019; Zhao et al., 2014). Bilinear interpolation in the GEE environment was used to interpolate the coarse resolution of GLDAS to 1 km spatial resolution, and the method was widely used to minimize the footprint impact of coarse resolution inputs (Ershadi et al., 2013; Zhang et al., 2019). The use of the GLDAS dataset is considered a good way to overcome the inadequacy of the observed dataset. Besides, the minimum temperature

(T$_{min}$), maximum temperature (T$_{max}$), water vapor pressure (P$_{wv}$), sunshine duration (SD), shortwave radiation (SW), and precipitation (P) gridded data at a spatial resolution of 1 km from the fourth version of the Daymet dataset (Daymet V4) (Thornton et al., 2020), derived from weather station data and various ancillary data sources, were also used in the Colorado River Basin.

2.2.2.2. Topographic data.
The topographic datasets used in this study include elevation (Ele), slope (Slo), and aspect (Asp) datasets. Elevation was obtained from the Shuttle Radar Topography Mission (SRTM) version 4 data (Jarvis et al., 2008) with a spatial resolution of 90 m. The slope and aspect datasets were generated based on this data using the spatial calculation method in the GEE environment (Gorelick et al., 2017).

2.2.2.3. Geographic location.
The geographic location data used in this study include longitude and latitude datasets at 1 km spatial resolution generated by calling the longitude and latitude calculation module in the GEE environment (Gorelick et al., 2017).

2.2.3. Land cover

Landcover data is derived from the European Space Agency (ESA) Climate Change Initiative Land Cover (ESA-CCI-LC) (Bontemps et al., 2012) with a spatial resolution of 300 m. This data extends from 1992 to 2019 with 37 land cover classes (ESA, 2015; ESA, 2018), and it is widely used in land cover transitions (Liu et al., 2018), land cover change (Mousivand and Arsanjani, 2019), gross and net land cover changes in the main plant functional types (Li et al., 2018b), hydrological modeling and climate change studies (Ayehu et al., 2020; Clark et al., 2017; Georgievski and Hagemann, 2019; Jaafar et al., 2019; Li et al., 2018a; Nkiaka et al., 2018; Osei et al., 2019; Tan et al., 2021). ESA-CCI-LC contains rainfed agriculture, mosaic agriculture, irrigated agriculture, and settlement, which is useful for quantifying the impact of the cultivation, irrigation, and urban construction on water consumption. Referring to the reclassification of CCI-LC by others (Mousivand and Arsanjani, 2019; Reinhart et al., 2021) and considering the natural and anthropogenic use attributes of land cover, the original LULC class values of CCI-LC were classified into the following six classes (Supplementary Table 1): Class 1: rainfed agriculture; Class 2: mosaic agriculture; Class 3: irrigated agriculture; Class 4: settlement; Class 5: water; and Class 6: natural land cover.

2.3. Method

2.3.1. Conceptual framework

Normally, in the absence of human intervention, ET from natural land cover is generated by natural factors, such as meteorological, topographic, geographic factors. When the land cover types are converted from natural land cover to managed land use due to human activities, such as forest to cropland, the ET drivers will extend from the natural factors to natural and anthropogenic factors. Therefore, ET from managed land use can be decomposed into natural ET (ET$_n$) and human-induced ET (ET$_h$) (Wu et al., 2018), with the following equation:

$$ET_t = ET_n + ET_h \tag{1}$$

where ET$_t$ is the total ET of managed land use, ET$_n$ is the ET fraction of managed land use contributed by natural factors, and ET$_h$ is the ET fraction

of managed land use caused by different human activities in the watershed, such as cultivation, irrigated, impervious surface building. Therefore, ET_h can be expressed as:

$$ET_h = ET_t - ET_n \qquad (2)$$

If ET_h is greater than 0, human activities on managed land use increase water consumption; otherwise, human activities on managed land use decrease water consumption. Assuming that ET_n can be determined by meteorology (Met), topography (Top), and geographic location (Geo) without anthropogenic disturbances, ET_n is characterized as follows:

$$ET_n = F(Met, Top, Geo) \qquad (3)$$

To predict the ET_n for managed land use, this study first distinguishes land cover in the study area into natural and human-managed land cover types according to land use (Section 2.2.3) and then divide the ET, Met, Top, and Geo datasets into two parts corresponding to natural land cover and human-managed land cover types. Without considering the interaction between natural and human-managed land cover types, this study assumes that natural forces generate ET of natural land cover types exclusively. It is worth noting that pixels with annual P > ET refer to net water producer of natural land covers and ensure that all ET is derived from P without the influence of human activities through irrigation, groundwater recharge, seepage, or base flow (Bastiaanssen et al., 2014; van Eekelen et al., 2015). Therefore, those pixels of natural land covers with annual P < ET were excluded from the ET separation modeling. This study developed the ET_n prediction model based on this assumption by exploring the links between Met, Top, and Geo parameters and ET corresponding to natural land cover types by RFR algorithm. RFR is an ensemble learning method with solid data mining capability, which trains multiple weak models and packages them to form a robust model (Breiman, 2001). The established prediction model predicts ET_n of human-managed land cover types (rainfed, mosaic, irrigated agriculture, and settlement) using Met, Top, and Geo

parameters corresponding to the human-managed land cover types as inputs. Finally, the total ET of the human-managed land cover type is subtracted from the predicted ET_n to obtain the ET_h, thus separating ET_n and ET_h of the human-managed land cover types. The study idea is illustrated in Fig. 2.

2.3.2. ET separation modeling

Meteorological parameters are key factors influencing ET. ET is closely related to net radiation, air temperature, water vapor pressure, and normalized vegetation index. For example, the total annual net radiation, average annual precipitation, and average annual air temperature are the main factors affecting annual ET and explain 84% of the spatial variation of the annual ET in China (Zheng et al., 2016). The interannual variation of ET was closely related to potential ET and precipitation (Zhang et al., 2016), with potential ET being the largest factor affecting ET when the aridity index ≤ 0.76 and precipitation being the largest factor affecting ET when the aridity index > 0.76. In the Haihe Basin, the trend of annual ET was closely related to vegetation cover, wind speed, and air pressure (Yan et al., 2018). ET was closely related to wind speed and vegetation cover in the Loess Plateau, followed by atmospheric pressure, air humidity, precipitation, sunshine hours, and temperature (Ma et al., 2019). Meteorological conditions are closely linked to atmospheric conditions and are strongly influenced by topography and geographical location. Therefore, this study first explores the intrinsic links between annual Met (P, LWdown, Tair, DWdown, Wind, Psurf, Qair), Top (Ele, Slo, and Asp), Geo (Lon, and Lat), and ET from natural land cover to construct the ET_n prediction model. Then use this model to predict ET_n of human-managed land cover types. Finally, obtain the ET_h of human-managed land cover types according to Eq. (2). This study illustrates our methodology at Colorado, Blue Nile, and Heihe Basins in the following four steps using 2017 data (Section 2.2) as an example (Fig. 3).

Step 1: Divide the land cover into natural and human-managed land cover categories (Section 2.2.3), based on which ET and its corresponding annual Met factors (P, LWdown, Tair, DWdown, Wind, Psurf, Qair), Top
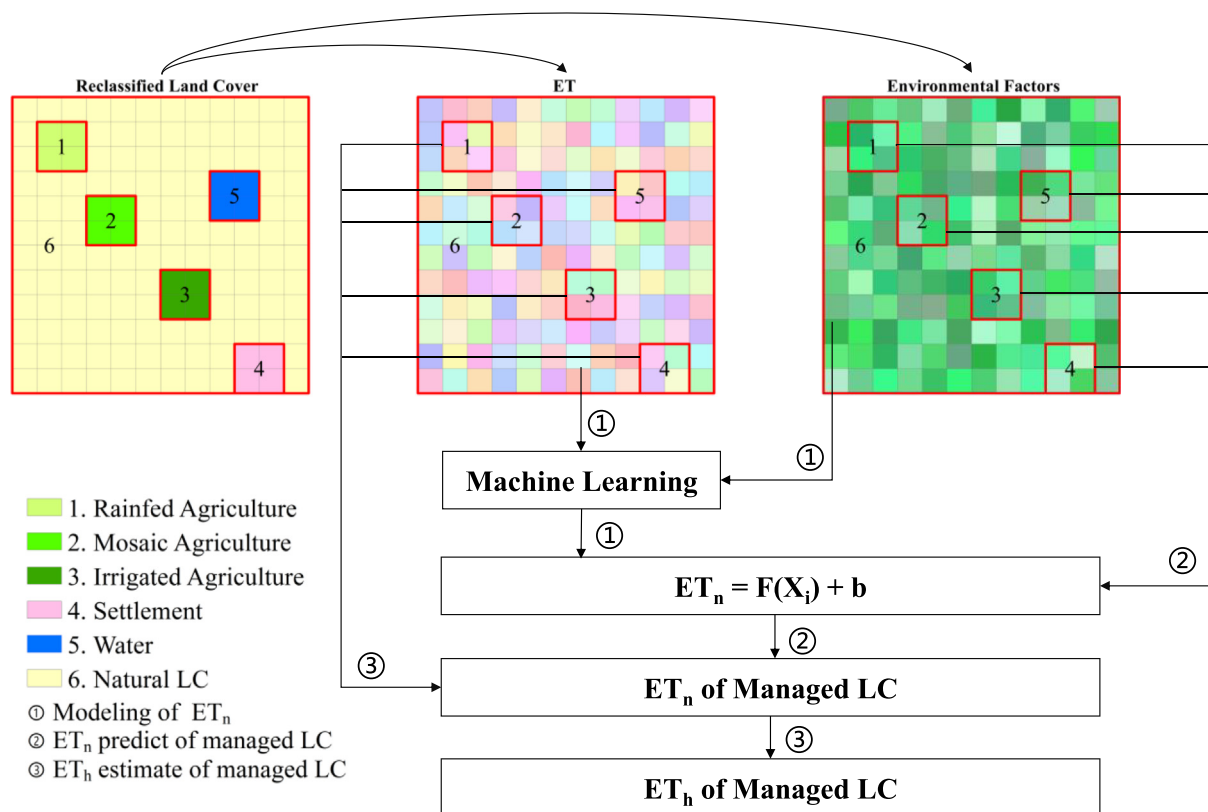

Fig. 2. Conceptual framework of the method on the separation of natural ET and anthropogenic ET of human-managed land cover types.
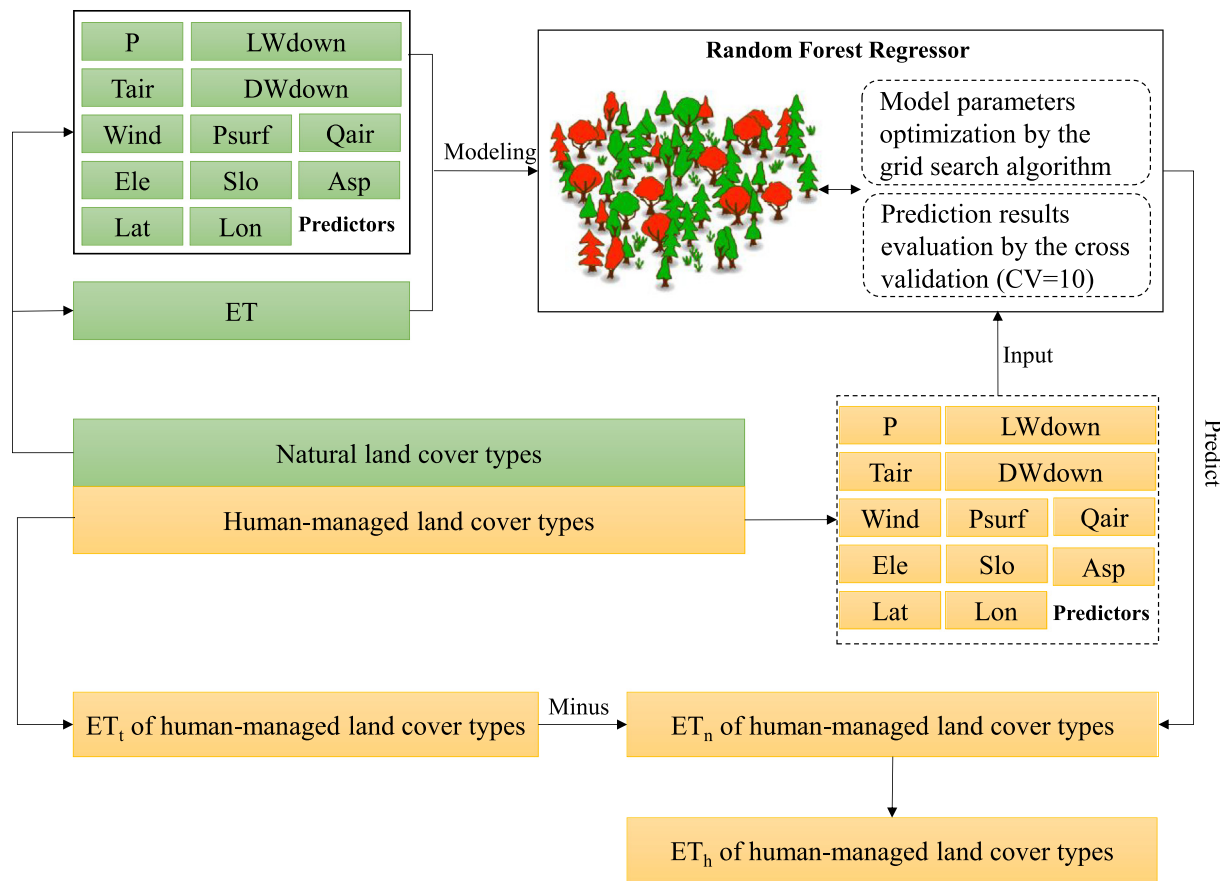
Fig. 3. Flowchart of ET_n and ET_h separation of human-managed land cover types.

factors (Ele, Slo, Asp), and Geo factors (Lon and Lat) datasets were also divided into their corresponding natural and managed categories.

Step 2: Based on the natural land cover categories with their corresponding ET and environmental variables data, the RFR is employed to mine the intrinsic links between ET_n and annual-Met, Top, and Geo factors to build ET_n prediction model (GLDAS ET_n model).

$$ET_n = F(P, LWdown, Tair, DWdown, Wind, Psurf, Qair, Ele, Slo, Asp, Lat, Lon)$$
$$(4)$$

These data were split into training and validation groups at 75% and 25%, respectively. The validation sizes (25% of the total size) for Colorado, Blue Nile, and Heihe Basins in this study were 59,883, 13,577, and 18,893, respectively, ensuring the credibility of the machine learning-based ET prediction models in the three basins. The grid search algorithm with a cross-validation approach (Pedregosa et al., 2011) is employed to optimize the hyper-parameters of the RFR algorithm (e.g., Elnashar et al., 2020; Jing et al., 2016; Jing et al., 2017).

Step 3: The ET_n prediction model was used to predict the ET_n caused by natural factors on managed land use using the corresponding predictor variables for human-managed land cover types.

Step 4: Subtract the ET_n of the managed land vegetation predicted in Step 3 from the total ET of the managed land cover in Step 1 to calculate the ET_h of the human-managed land cover types.

2.3.3. Model's performance assessment

The ET_n predicted results were assessed by five statistical indices (Su et al., 2008; Zhao et al., 2017), including the correlation coefficient (R^2), mean absolute error (MAE), root mean square error (RMSE), relative bias (RB), and Nash–Sutcliffe coefficient of efficiency (NSE). From Step 2 (Section 2.3.2), predicted ET_n is the ET predicted from environmental

variables using RFR, while the reference ET is the ET of the validation group. R^2 represents a linear correlation between predicted ET_n and the reference ET. RB is the relative difference between predicted ET_n and the reference ET. RMSE is the error between ET_n and reference ET (mm yr^{-1}). The Nash-Sutcliffe efficiency coefficient (NSE) is used to assess the efficiency of ET_n prediction models. The perfect value of R^2, RB, RMSE, MAE, and NSE are 1, 0, 0, 0, and 1, respectively.

3. Results

3.1. ET separation

Based on the framework presented in Fig. 3, this study generated ET_t, ET_n, and ET_h for four management types, namely rainfed agriculture, mosaic agriculture, irrigated agriculture, and settlement, for the Colorado River Basin, Blue Nile Basin, and Heihe Basin in 2017 (Fig. 4).

In the Colorado River Basin, the contribution of human activities to water consumption in rainfed agriculture, mosaic agriculture, and settlement all show an increasing effect. The rates of ET_t for these three types were 500.8 mm yr^{-1}, 552.4 mm yr^{-1}, and 325.6 mm yr^{-1}, corresponding to the total water consumption of 9676×10^6 m^3 yr^{-1}. The rates of ET_n for these three managed land uses are 308.0 mm yr^{-1}, 237.8 mm yr^{-1}, and 182.4 mm yr^{-1}, corresponding to the total water consumption of 4482×10^6 m^3 yr^{-1}, representing 46.32% of the total water consumption of the three managed land uses. The rates of ET_h is 192.8 mm yr^{-1}, 314.6 mm yr^{-1}, and 143.2 mm yr^{-1}, corresponding to the total water consumption of 5194×10^6 m^3 yr^{-1}, representing 53.68% of the total water consumption of the three managed land uses.

In the Blue Nile Basin, the contribution of human activities to water consumption in rainfed agriculture, mosaic agriculture, irrigated agriculture, and settlement all show an increasing effect. The rates of ET_t for rainfed
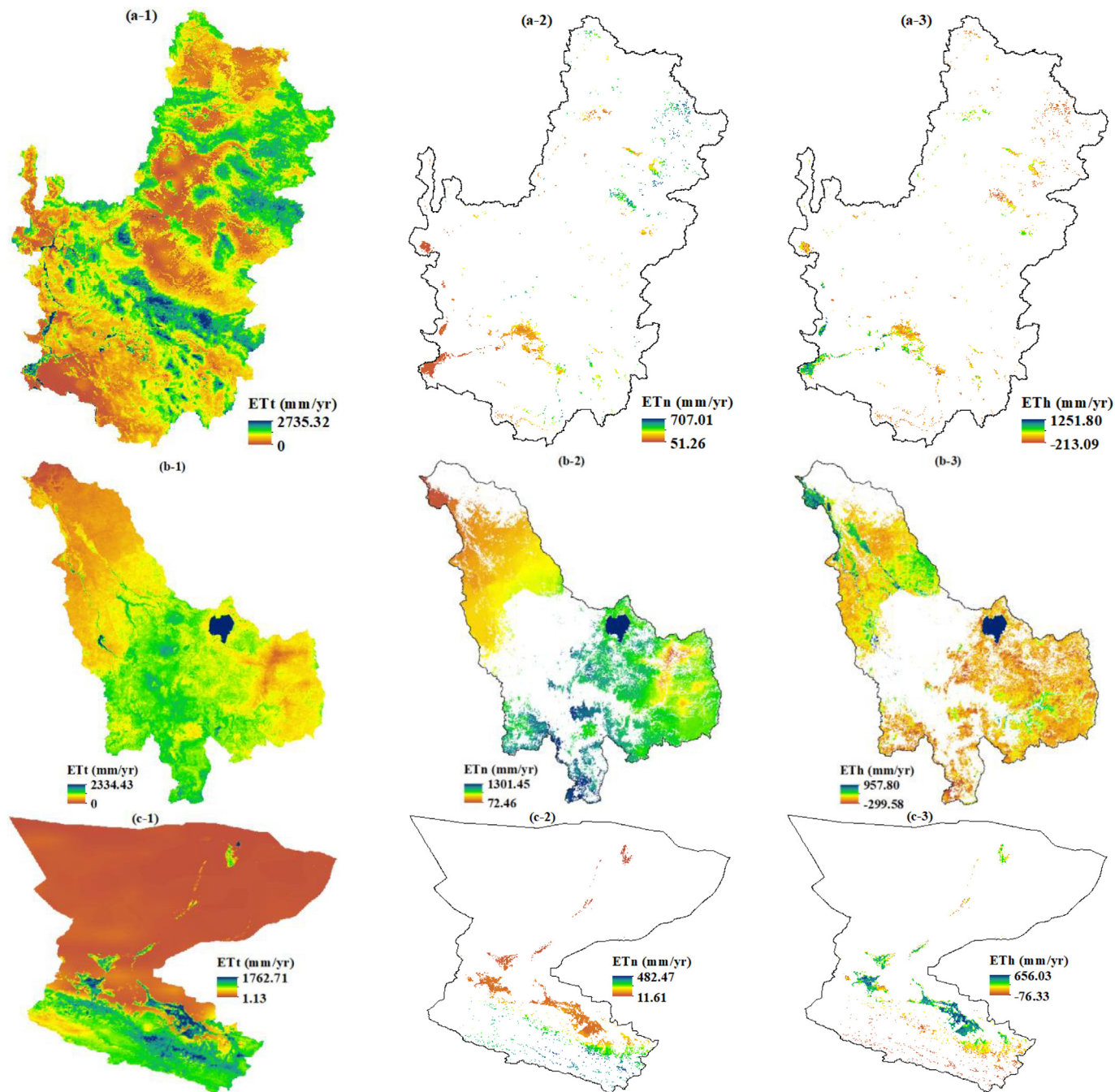
Fig. 4. Colorado River Basin (a), Blue Nile Basin (b), and Heihe Basin (c); total ET (1: left), natural ET (2: middle), and anthropogenic ET (3: right).

agriculture, mosaic agriculture, irrigated agriculture, and settlement were 686.4 mm yr^{-1}, 753.1 mm yr^{-1}, 513.4 mm yr^{-1}, and 509.5 mm yr^{-1}, respectively, with estimated total water consumption of 91,819 × 10^6 m^3 yr^{-1}. Human activities increase the rates of ET$_t$ of the four managed land uses by 44.6 mm yr^{-1}, 16.4 mm yr^{-1}, 163.9 mm yr^{-1}, and 98.2 mm yr^{-1}, respectively, totaling 5640 × 10^6 m^3 yr^{-1} approaching 6.14% of the total water consumption while ET$_n$ counts for 93.86% of the total water consumption.

In the Heihe Basin, the impact of human activities on water consumption in rainfed agriculture, mosaic agriculture, irrigation agriculture, and settlement is reflected in a strong increasing effect. The ET$_t$ rates for four managed land uses were 432.0 mm yr^{-1}, 360.3 mm yr^{-1}, 420.9 mm yr^{-1}, and 249.5 mm yr^{-1}, respectively, corresponding to the total water consumption of 2982 × 10^6 m^3 yr^{-1}. The ET$_n$ rates for the four managed land uses were134.0 mm yr^{-1}, 185.8 mm yr^{-1}, 66.0 mm yr^{-1}, and

60.5 mm yr^{-1}, respectively, corresponding to 1000 × 10^6 m^3 yr^{-1}, accounting for 33.53% of the total water consumption. The rates of ET$_h$ for the four managed land uses were 298.0 mm yr^{-1}, 174.4 mm yr^{-1}, 354.9 mm yr^{-1}, and 189.1 mm yr^{-1}, respectively, corresponding to the total water consumption of 1982 × 10^6 m^3 yr^{-1}, accounting for 66.47% of the total water consumption of the four managed land uses.

3.2. Model performance

This study developed three ET$_n$ prediction models at 1 km driven by 12 environmental predictors in Colorado, Blue Nile, and Heihe Basins. All indicators are showed that three ET$_n$ prediction models had good predictive performance (Fig. 5). The predicted results of ET$_n$ has an excellent correlation with remote sensing ET result; both R^2 and NSE of the Colorado River Basin, Blue Nile Basin, and Heihe Basin are 0.96, 0.98, and 0.99,
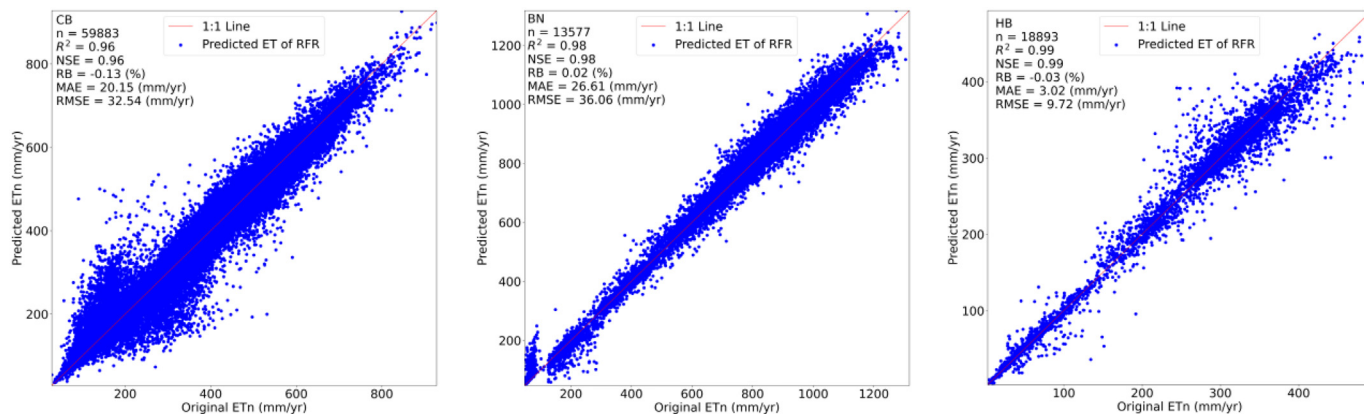
Fig. 5. Cross-validation of ET_n prediction in Colorado River Basin (left), Blue Nile Basin (middle), and Heihe Basin (right) in 2017.

respectively, implying that the predicted results of ET_n matched well with the remote sensing ET. A minimal magnitude of relative bias (RB) was observed in the Colorado River Basin (RB = −0.13%), Blue Nile Basin (RB = 0.02%), and Heihe Basin (RB = −0.03%). The minor errors are observed by MAE, and RMSE in the Colorado River Basin (MAE = 20.15 mm yr^{-1}, RMSE = 32.54 mm yr^{-1}), Blue Nile Basin (MAE = 26.61 mm yr^{-1}, RMSE = 36.06 mm yr^{-1}), and Heihe Basin (MAE = 3.06 mm yr^{-1}, RMSE = 9.72 mm yr^{-1}), respectively. Besides, the scatter points were almost always distributed around the 1:1 line, indicating the good performance of the ET_n model developed in the three basins. The excellent performance of the three ET_n models confirms the validity of the ET_n prediction model proposed in this study to predict the annual ET caused by natural factors using annual-Met, Top, and Geo datasets.

This study assessed the importance of 12 environmental predictors in the ET_n prediction model for the Colorado, Blue Nile, and Heihe Basins assessed by RFR (Table 3). The importance of the environmental predictors in the natural ET prediction models varied with climate and regions. In the semi-arid Colorado River Basin, the top 5 environmental predictors were P, Qair, Ele, Lat, and Lon, accounting for 72.94%, 5.94%, 5.82%, 5.02%, and 2.88%, respectively. Similarly, in the arid Heihe Basin, P, Qair, Ele, Lat, and Lon were among the top 5 environmental predictors, but their weights on ETn were 95.08%, 1.61%, 0.95%, 0.84%, and 0.66%, respectively. Whereas in the humid Blue Nile basin, P, Qair, Wind, Ele, and Tair were ranked as the top 5 environmental predictors with weights of 69.88%, 17.94%, 2.66%, 2.21%, and 1.66%, respectively.

4. Discussions

This study proposed a framework for separating the contribution of natural and anthropogenic factors to ET of human-managed land cover types, effectively quantifying the contribution of natural processes and human

activities to ET from human-managed land cover types, and has been successfully demonstrated in the Colorado River Basin, Blue Nile Basin, and Heihe Basin. The method quantifies the amount of change in water consumption by human activities at the pixel level and can measure the water consumption effects of different human activities, supporting the regulation of water resources at the basin scale.

4.1. ET due to anthropogenic interventions

The variation in the magnitude of the anthropogenic ET is related to climate type, with all human-managed land cover types in the study area showing an increasing trend in total water consumption. The Colorado River Basin and the Heihe Basin are located in semi-arid and arid regions, respectively, and human activities in both basins have a more significant effect on increased ET than in the Blue Nile Basin, where 64% of the total area is located in the humid region (Elnashar et al., 2022). Previous studies supported our findings (Castle et al., 2016; Hurni et al., 2005; Zou et al., 2017). A study from the Heihe Basin showed that human activities were the leading cause of the increase in ET in agricultural areas from 1984 to 2014 at rates of 53.86–60.93% (Zou et al., 2017). Our result in Table 2 showed that the human activities in the Heihe Basin increased the total ET of agricultural areas by 66.47%, which is slightly higher than the findings of Zou et al. (2017), indicating a more profound impact of human activities on agricultural water consumption in Heihe Basin. A study from the Colorado River Basin indicated that human activities increased water consumption, the trend is consistent with our finding (Castle et al., 2016). The study estimated that the average annual anthropogenic ET of the entire Colorado River Basin was 21.0 ± 12.3 km^3 yr^{-1} from 2003 to 2013, and our study estimated that the annual anthropogenic ET was 5.194 km^3 yr^{-1} in 2017. It is worth noting that the results of Castle et al. (2016) are higher than our results mainly because it was estimated using GRACE data, which

Table 2
ET_t, ET_n, and ET_h for human-managed land cover types in 2017.

Basin	LULC	Area	ET_t		ET_n		ET_h	
		km^2	mm	10^6 m^3	mm	10^6 m^3	mm	10^6 m^3
Colorado River	Rainfed agriculture	1095	500.8	548.4	308.0	337.3	192.8	211.1
Colorado River	Mosaic agriculture	13,524	552.4	7470.8	237.8	3216.4	314.6	4254.5
Colorado River	Irrigated agriculture	–	–	–	–	–	–	–
Colorado River	Settlement	5089	325.6	1657.1	182.4	928.2	143.2	728.8
Blue Nile	Rainfed agriculture	60,034	686.4	41,208.5	641.8	38,532.0	44.6	2676.5
Blue Nile	Mosaic agriculture	58,787	753.1	44,272.0	736.6	43,305.2	16.4	966.8
Blue Nile	Irrigated agriculture	11,933	513.4	6126.0	349.5	4170.3	163.9	1955.7
Blue Nile	Settlement	417	509.5	212.5	411.3	171.5	98.2	41.0
Heihe	Rainfed agriculture	2661	432.0	1149.5	134.0	356.5	298.0	793.0
Heihe	Mosaic agriculture	2727	360.3	982.5	185.8	506.8	174.4	475.7
Heihe	Irrigated agriculture	1927	420.9	811.1	66.0	127.2	354.9	683.9
Heihe	Settlement	154	249.5	38.4	60.5	9.3	189.1	29.1

Table 3
Features importance in the regression model by RFR in 2017.

Basin	Lon	Lat	Asp	Slo	Ele	Tair	Psurf	Qair	SWdown	P	LWdown	Wind
Colorado	2.88	5.02	0.56	1.43	5.82	1.25	1.07	5.94	1.37	72.94	0.53	1.20
Blue Nile	1.62	1.07	0.23	0.95	2.21	1.66	0.36	17.94	0.78	69.88	0.65	2.66
Heihe	0.66	0.84	0.14	0.16	0.95	0.13	0.04	1.61	0.05	95.08	0.30	0.03

Table 4
ET_t, ET_n, and ET_h (mm yr^{-1}) from Daymet over Colorado River Basin and WAPOR ET over the Blue Nile Basin in 2017.

LULC	Daymet (Colorado River Basin)			WAPOR (Blue Nile Basin)		
	ET_t	ET_n	ET_h	ET_t	ET_n	ET_h
Rainfed agriculture	500.8	298.6	202.3	781.5	695.7	85.8
Mosaic agriculture	552.1	216.8	335.3	856.0	797.5	58.5
Irrigated agriculture	–	–	–	786.8	402.1	384.7
Settlement	325.0	175.4	149.6	546.7	456.2	90.4

4.2. Uncertainties of ET separation model

To test the effects of different meteorological data sources on the ET_n prediction model, Daymet datasets were used with the same Top and Geo factors as Fig. 5 to build a new ET_n prediction model (Daymet ET_n model) over the Colorado River Basin. From Fig. 5 (left) compared to Fig. 6 (left), the two results are very similar, with the same R^2 and NSE values; however, the GLDAS ET_n model returned lower MAE and RMSE than the Daymet ET_n model, for that this study selected the GLDAS ET_n model to predict the 2017 ET_n of Colorado River Basin. ET_n and ET_h from Daymet ET_n model (Table 4) and GLDAS ET_n model (Table 2) are very close, in which ET_h predicted by the Daymet ET_n model was 9.5 mm yr^{-1} and 20.7 mm yr^{-1} and 6.4 mm yr^{-1} lower for rainfed, mosaic, and settlement than that predicted by the GLDAS ET_n model.

In addition, as ET represents the combined effect of natural and anthropogenic water consumption, improving the accuracy and spatial resolution of remotely sensed ET is also one of the keys to better differentiating between ET's natural and anthropogenic contributions. Herein, we changed the ET data of the Blue Nile Basin to WAPOR ET data (FAO, 2020). The R^2 and NSE for the ET_n prediction model of the synthesized ET from Fig. 5 (right) and the WAPOR ET from Fig. 6 (right) are the same, but the MAE and RMSE metrics showed that the synthesized ET-based prediction model provided reduced biases and higher accuracy. In addition, similar to the synthesized ET results (Table 2; Blue Nile), the WAPOR ET data (Table 4) reveal that human activities also increase ET compared to the natural state. These results confirm the stability of the regression model in ET separation for extracting human activity's direction on ET. The difference is found in the magnitude of the human-induced ET, implying that these differences are due to the ET data source and not the regression model. A recent study by McNamara et al. (2021) confirmed the superiority of PML over WAPOR in the Nile Basin. Current ET products have some uncertainty, and there is a need to develop a more accurate method of ET monitoring, which is why integrated ET was chosen for this study, as it combines the advantages of PML and SSEBop products.
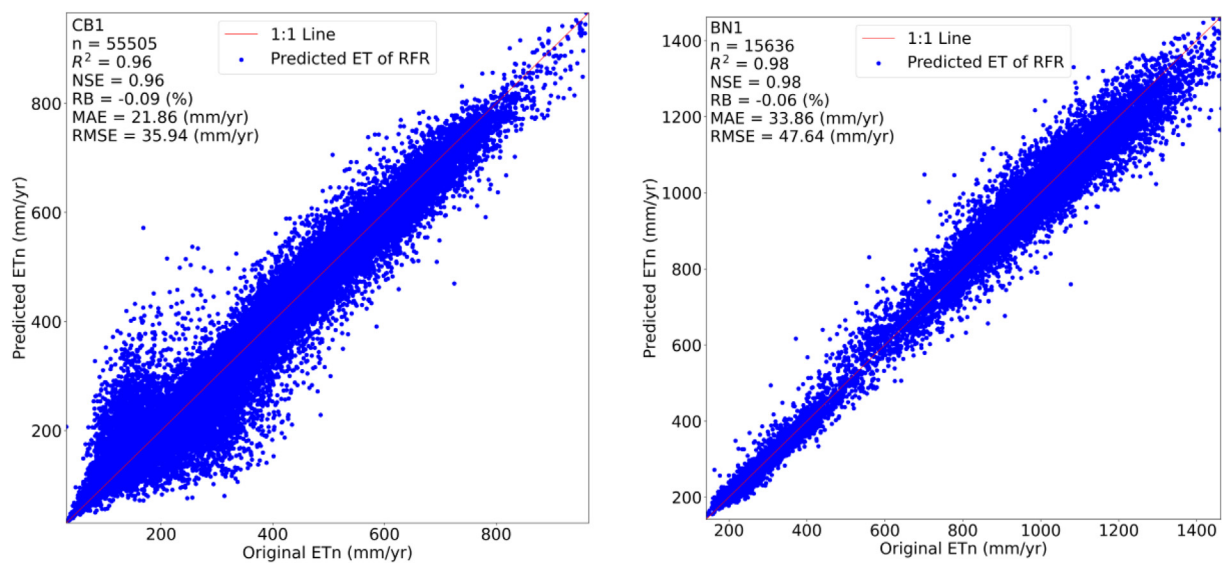
included water loss due to ET from reservoirs and interbasin water allocation (Christensen et al., 2004). When added to 5.43 km^3 yr^{-1} of annual water allocated to California (outside the Colorado River Basin) (Swanson et al., 2021) and 1.85 km^3 yr^{-1} of reservoirs ET (Castle et al., 2016), anthropogenic ET of Colorado in 2018 is 12.474 km^3 yr^{-1} which is comparable to the results of Castle et al. (2016). Therefore, all types of human activities in arid and semi-arid areas have to consider their impact on the availability of regional water resources. The findings that human activities in arid and semi-arid regions have increased water consumption was also supported by other previous studies, such as the 'Grain to Green' revegetation program on the Loess Plateau in China caused regional water consumption to approach the limits of sustainable water resources (Feng et al., 2016). The expansion of irrigated arable land has increased water consumption, resulting in the rapid shrinkage of Lake Ebinur (Zeng et al., 2019). In the Blue Nile Basin, Table 2 showed that the human activities also increased the ET of all managed land covers, but much less than the human-induced ET in the Colorado River Basin and Heihe Basin. This can be attributed to the predominantly humid climate of the Blue Nile basin, where abundant precipitation provides abundant soil water for crop growth without the need for additional irrigation water (Camberlin, 2009).

Fig. 6. Performance validation of ET_n based on Daymet over Colorado River Basin (left) and WAPOR ET over the Blue Nile Basin (right) in 2017.

4.3. Implications of the proposed framework

The ET separation framework proposed in this study provides an effective way to understand the impact of changing meteorological and climatic conditions on ET and can benefit the regulation of the impact of human activities on total water consumption at a basin scale. The geographical locates and topographic variables in the ET_n prediction model are static input variables; in contrast, the meteorological variables are dynamic input variables, so the impact of changing meteorological conditions on ET can be assessed by inputting meteorological data from different years. On the other hand, the impact of climate change on water consumption can also be predicted through inputting meteorological data under different climate change scenarios using the proposed framework. Increased water withdrawals upstream usually lead to the reduction of downstream water supply, especially in drought years (Nikiel and Eltahir, 2021; Yoon et al., 2015); therefore, the optimal allocation of water resources in arid and semi-arid regions is crucial for sustainable development of dryland ecosystems, food production, biodiversity conservation and ecosystems sustainable management (Marques et al., 2016; McClain, 2013). The proposed framework quantifies the water consumption of different human-managed land covers, evaluating the reasonable scale of agricultural development at the basin scale, optimizing planting structures, identifying irrigation methods to reduce water consumption and also providing opportunities for transboundary water cooperation by separating natural ET from anthropogenic ET. Hence, the proposed framework can help target areas where effective ways to reduce agricultural water consumption should be implemented (Elnashar et al., 2021a; Mojid and Mainuddin, 2021) for producing more food with less water through increased crop water productivity (Cai et al., 2011; Nhamo et al., 2016). For example, land use change and water resources management through reservoir regulation have had a significant impact on reducing evapotranspiration (Chen et al., 2019a), on-farm strategies reduced water input in irrigated crops (Bouman et al., 2007; Tabbal et al., 2002), shifting planting date as climate change adaptation strategy to reduce water use (Acharjee et al., 2019), or water savings using greenhouses crop production (O'Connor and Mehta, 2016).

4.4. Advantages and limitations

Compared to the ET separation method coupled with GRACE data and hydrological models (Castle et al., 2016; Pan et al., 2017), the method proposed in this study has a major improvement in spatial resolution and differentiation of human contributions. One is to quantify ET's perturbation by human activities at a finer scale (1 km). The other is to quantify the impact of different human activity behaviors on ET, such as rainfed agricultural cultivation, irrigated agricultural cultivation, and settlement building. Compared with the method based on the spatial interpolation of ET of uncultivated cropland proposed by Wu et al. (2018), the present method overcomes the uncertainty problem caused by the sparse interpolation of the number of uncultivated cropland. Compared to the WA+ method proposed by FAO (Karimi et al., 2013), the FAO method can broadly distinguish between types of ET based on land cover use patterns but cannot quantify the contribution of natural and human activities to ET in human-managed land cover types. In contrast to the method proposed by Zou et al. (2017), which uses statistical methods to differentiate between human activities and climate change impacts on ET annual change, our approach can identify the contribution of human activities and the effects of natural forcing on ET itself.

Applying the ET contribution separation method proposed in this study also needs to be supported by fine resolution and high-precision land cover data (e.g., Nabil et al., 2021). With the emergence of land cover products with finer resolution, richer types and better accuracy, and the emergence of remote sensing ET products with higher accuracy and finer resolution, the ET separation method proposed in this study can more accurately quantify the contribution of different human activity behaviors to water consumption, and thus provide more robust support for basin-scale water

consumption management and regulation. In particular, crop structure, irrigation, and rainfed, different human practices greatly impact ET (Zou et al., 2017), so they need to be mapped at a finer scale to quantitatively assess the impact of different agricultural interventions on water consumption. For example, the difference in water consumption due to human activities between different climatic, soil conditions, and irrigation practices for the same crop, and the difference in water consumption for different crops under the same or different human intervention scenarios. This plays an essential role in developing agricultural water conservation measures, particularly in arid or semi-arid basins like the Heihe or Colorado River Basin. Copernicus CORINE Land Cover of ESA (Feranec et al., 2010; Kallimanis and Koutsias, 2013) provides different artificial land covers augmented with more specific ET data (e.g., Wang et al., 2021) can be used to identify better the impact of different human activities on water consumption in the future.

5. Conclusions

This study proposed a framework coupled with satellite-based ET, land cover, environmental factors (meteorological, topographic, and geolocation data), and machine learning for separating the contribution of human activities and natural forces to ET of human-managed land cover types based on the drivers of ET of human-managed land cover types. Taking the year 2017 as an example, the models built in the Colorado River Basin, Blue Nile Basin, and Heihe Basin all had good agreements in predicting natural ET, with R^2 and NSE above 0.95 and RB within <1%. The framework effectively distinguished the contribution of natural drivers and human activities to ET from rainfed agriculture, mosaic agriculture, irrigated agriculture, and settlement. In the semi-arid Colorado River Basin and the arid Heihe Basin, human activities increased ET in all four human-managed land cover types approaching 53.68% and 66.47%, respectively, much more than in the Blue Nile Basin, where the human activities contributed 6.14% to the total ET. Human activities that occur in drier basins tend to increase water depletion more than in wetter basins, and the proposed ET separation framework provides a new tool for analyzing the impact of climate change and human activities on ET, benefiting the sustainable use and management of soil and water resources in the basin. The concept could be applied in similar areas, given that it depends upon free and open access data and processing environment.

Supplementary data to this article can be found online at https://doi.org/10.1016/j.scitotenv.2022.153726.

CRediT authorship contribution statement

Declaration of competing interest

The authors declare that they have no known competing financial interests or personal relationships that could have appeared to influence the work reported in this paper.

Acknowledgements

the meteorological data covering Colorado, Blue Nile, and Heihe Basin; Oak Ridge National Laboratory of the United States for providing the meteorological data in Colorado.

References

Acharjee, T.K., van Halsema, G., Ludwig, F., Hellegers, P., Supit, I., 2019. Shifting planting date of boro rice as a climate change adaptation strategy to reduce water use. Agric. Syst. 168, 131–143.

Ayehu, G., Tadesse, T., Gessesse, B., 2020. Monitoring residual soil moisture and its association to the long-term variability of rainfall over the upper Blue Nile Basin in Ethiopia. Remote Sens. 12, 2138.

Badgley, G., Fisher, J.B., Jiménez, C., Tu, K.P., Vinukollu, R., 2015. On uncertainty in global terrestrial evapotranspiration estimates from choice of input forcing datasets. J. Hydrometeorol. 16, 1449–1455.

Bastiaanssen, W.G.M., Karimi, P., Rebelo, L.-M., Duan, Z., Senay, G., Muthuwatte, L., et al., 2014. Earth observation based assessment of the water production and water consumption of Nile basin agro-ecosystems. Remote Sens. 6, 10306–10334.

Bontemps, S., Defourny, P., Brockmann, C., Herold, M., Kalogirou, V., Arino, O., 2012. New global land cover mapping exercise in the framework of the ESA climate change initiative. 2012 IEEE International Geoscience and Remote Sensing Symposium.

Bouman, B.A.M., Feng, L., Tuong, T.P., Lu, G., Wang, H., Feng, Y., 2007. Exploring options to grow rice using less water in northern China using a modelling approach: II. Quantifying yield, water balance components, and water productivity. Agric. Water Manag. 88, 23–33.

Breiman, L., 2001. Random forests. Mach. Learn. 45, 5–32.

Budyko, M.I., 1974. Climate and Life. Academic, Orlando, Fla.

Cai, X., Molden, D., Mainuddin, M., Sharma, B., M-u-D, Ahmad, Karimi, P., 2011. Producing more food with less water in a changing world: assessment of water productivity in 10 major river basins. Water Int. 36, 42–62.

Camberlin, P., 2009. Nile Basin climates. In: Dumont, H.J. (Ed.), The Nile: Origin, Environments, Limnology and Human Use. Springer Netherlands, Dordrecht, pp. 307–333.

Castle, S.L., Reager, J.T., Thomas, B.F., Purdy, A.J., Lo, M.-H., Famiglietti, J.S., et al., 2016. Remote detection of water management impacts on evapotranspiration in the Colorado River basin. Geophys. Res. Lett. 43, 5089–5097.

Che, T., Li, X., Liu, S., Li, H., Xu, Z., Tan, J., et al., 2019. Integrated hydrometeorological, snow and frozen-ground observations in the alpine region of the Heihe River Basin, China. Earth Syst. Sci. Data 11, 1483–1499.

Chen, H., Zhang, W., Jafari Shalamzari, M., 2019. Remote detection of human-induced evapotranspiration in a regional system experiencing increased anthropogenic demands and extreme climatic variability. Int. J. Remote Sens. 40, 1887–1908.

Chen, Y., Li, B., Fan, Y., Sun, C., Fang, G., 2019b. Hydrological and water cycle processes of inland river basins in the arid region of Northwest China. J. Arid Land 11, 161–179.

Christensen, N.S., Lettenmaier, D.P., 2007. A multimodel ensemble approach to assessment of climate change impacts on the hydrology and water resources of the Colorado River basin. Hydrol. Earth Syst. Sci. 11, 1417–1434.

Christensen, N.S., Wood, A.W., Voisin, N., Lettenmaier, D.P., Palmer, R.N., 2004. The effects of climate change on the hydrology and water resources of the Colorado River basin. Clim. Chang. 62, 337–363.

Clark, R.A., Flamig, Z.L., Vergara, H., Hong, Y., Gourley, J.J., Mandl, D.J., et al., 2017. Hydrological modeling and capacity building in the Republic of Namibia. Bull. Am. Meteorol. Soc. 98, 1697–1715.

Döll, P., Siebert, S., 2002. Global modeling of irrigation water requirements. Water Resour. Res. 38, 8-1-8-10.

Elnashar, A., Zeng, H., Wu, B., Zhang, N., Tian, F., Zhang, M., et al., 2020. Downscaling TRMM monthly precipitation using Google earth engine and Google cloud computing. Remote Sens. 12, 3860.

Elnashar, A., Abbas, M., Sobhy, H., Shahba, M., 2021a. Crop water requirements and suitability assessment in arid environments: a new approach. Agronomy 11, 260.

Elnashar, A., Wang, L., Wu, B., Zhu, W., Zeng, H., 2021b. Synthesis of global actual evapotranspiration from 1982 to 2019. Earth Syst. Sci. Data 13, 447–480.

Elnashar, A., Zeng, H., Wu, B., Fenta, A.A., Nabil, M., Duerler, R., 2021c. Soil erosion assessment in the Blue Nile Basin driven by a novel RUSLE-GEE framework. Sci. Total Environ. 793, 148466.

Elnashar, A., Zeng, H., Wu, B., Gebremicael, T.G., Marie, K., 2022. Assessment of environmentally sensitive areas to desertification in the Blue Nile Basin driven by the MEDALUS-GEE framework. Sci. Total Environ. 815, 152925.

Ershadi, A., McCabe, M.F., Evans, J.P., Walker, J.P., 2013. Effects of spatial aggregation on the multi-scale estimation of evapotranspiration. Remote Sens. Environ. 131, 51–62.

ESA, 2015. Land Cover CCI Product User Guide Version 2.0. Available at:European Space Agency. http://maps.elie.ucl.ac.be/CCI/viewer/download.php. (Accessed 7 October 2018).

ESA, 2018. Land Cover CCI Product User Guide Version 2.0.7. Available at:European Space Agency. http://maps.elie.ucl.ac.be/CCI/viewer/download.php. (Accessed 7 October 2018).

FAO, 2020. WaPOR Quality Assessment: Technical Report on the Data Quality of the WaPOR FAO Database Version 2. Rome.

FAO, IHE Delft, 2020. Water Accounting in the Nile River Basin. FAO WaPOR Water Accounting Reports. Rome. https://doi.org/10.4060/ca9895en. (Accessed 21 January 2021).

Feng, X., Fu, B., Piao, S., Wang, S., Ciais, P., Zeng, Z., et al., 2016. Revegetation in China's loess plateau is approaching sustainable water resource limits. Nat. Clim. Chang. 6, 1019–1022.

Feranec, J., Jaffrain, G., Soukup, T., Hazeu, G., 2010. Determining changes and flows in european landscapes 1990–2000 using CORINE land cover data. Appl. Geogr. 30, 19–35.

Fisher, J.B., Melton, F., Middleton, E., Hain, C., Anderson, M., Allen, R., et al., 2017. The future of evapotranspiration: global requirements for ecosystem functioning, carbon and climate feedbacks, agricultural management, and water resources. Water Resour. Res. 53, 2618–2626.

Funk, C., Peterson, P., Landsfeld, M., Pedreros, D., Verdin, J., Shukla, S., et al., 2015. The climate hazards infrared precipitation with stations-a new environmental record for monitoring extremes. Sci. Data 2, 150066.

Georgievski, G., Hagemann, S., 2019. Characterizing uncertainties in the ESA-CCI land cover map of the epoch 2010 and their impacts on MPI-ESM climate simulations. Theor. Appl. Climatol. 137, 1587–1603.

Gorelick, N., Hancher, M., Dixon, M., Ilyushchenko, S., Thau, D., Moore, R., 2017. Google earth engine: planetary-scale geospatial analysis for everyone. Remote Sens. Environ. 202, 18–27.

Gosling, S.N., Arnell, N.W., 2016. A global assessment of the impact of climate change on water scarcity. Clim. Chang. 134, 371–385.

Ho, L., Alonso, A., Eurie Forio, M.A., Vanclooster, M., Goethals, P.L.M., 2020. Water research in support of the sustainable development goal 6: a case study in Belgium. J. Clean. Prod. 277, 124082.

Hoff, H., Falkenmark, M., Gerten, D., Gordon, L., Karlberg, L., Rockström, J., 2010. Greening the global water system. J. Hydrol. 384, 177–186.

Hurni, H., Tato, K., Zeleke, G., 2005. The implications of changes in population, land use, and land management for surface runoff in the upper Nile basin area of Ethiopia. Mt. Res. Dev. 25, 147–154.

Jaafar, H.H., Ahmad, F.A., El Beyrouthy, N., 2019. GCN250, new global gridded curve numbers for hydrologic modeling and design. Sci. Data 6, 145.

Jaramillo, F., Destouni, G., 2015. Local flow regulation and irrigation raise global human water consumption and footprint. Science 350, 1248–1251.

Jarvis, A., Reuter, H.I., Nelson, A., Guevara, E., 2008. Hole-filled SRTM for the Globe Version 4. Available from the CGIAR-CSI SRTM 90m Database.

Jing, W., Yang, Y., Yue, X., Zhao, X., 2016. A comparison of different regression algorithms for downscaling monthly satellite-based precipitation over North China. Remote Sens. 8, 835.

Jing, W., Zhang, P., Jiang, H., Zhao, X., 2017. Reconstructing satellite-based monthly precipitation over Northeast China using machine learning algorithms. Remote Sens. 9, 781.

Kallimanis, A.S., Koutsias, N., 2013. Geographical patterns of Corine land cover diversity across Europe: the effect of grain size and thematic resolution. Prog. Phys. Geogr. 37, 161–177.

Kang, E., Cheng, G., Lan, Y., Jin, H., 1999. A model for simulating the response of runoff from the mountainous watersheds of inland river basins in the arid area of Northwest China to climatic changes. Sci. China Ser. D Earth Sci. 42, 52–63.

Karimi, P., Bastiaanssen, W.G.M., Molden, D., 2013. Water accounting plus (WA+) – a water accounting procedure for complex river basins based on satellite measurements. Hydrol. Earth Syst. Sci. 17, 2459–2472.

Kim, S., Anabalón, A., Sharma, A., 2021. An assessment of concurrency in evapotranspiration trends across multiple global datasets. J. Hydrometeorol. 22, 231–244.

Leng, G., Huang, M., Tang, Q., Gao, H., Leung, L.R., 2014. Modeling the effects of groundwater-fed irrigation on terrestrial hydrology over the conterminous United States. J. Hydrometeorol. 15, 957–972.

Leng, G., Huang, M., Tang, Q., Leung, L.R., 2015. A modeling study of irrigation effects on global surface water and groundwater resources under a changing climate. J. Adv. Model. Earth Syst. 7, 1285–1304.

Li, S., Yang, H., Lacayo, M., Liu, J., Lei, G., 2018. Impacts of land-use and land-cover changes on water yield: a case study in Jing-Jin-Ji, China. Sustainability 10, 960.

Li, W., MacBean, N., Ciais, P., Defourny, P., Lamarche, C., Bontemps, S., et al., 2018b. Gross and net land cover changes in the main plant functional types derived from the annual ESA CCI land cover maps (1992–2015). Earth Syst. Sci. Data 10, 219–234.

Liu, X., Yu, L., Si, Y., Zhang, C., Lu, H., Yu, C., et al., 2018. Identifying patterns and hotspots of global land cover transitions using the ESA CCI land cover dataset. Remote Sens. Lett. 9, 972–981.

Ma, Z., Yan, N., Wu, B., Stein, A., Zhu, W., Zeng, H., 2019. Variation in actual evapotranspiration following changes in climate and vegetation cover during an ecological restoration period (2000–2015) in the Loess Plateau, China. Sci. Total Environ. 689, 534–545.

Mao, J., Fu, W., Shi, X., Ricciuto, D.M., Fisher, J.B., Dickinson, R.E., et al., 2015. Disentangling climatic and anthropogenic controls on global terrestrial evapotranspiration trends. Environ. Res. Lett. 10, 094008.

Marques, M.J., Schwilch, G., Lauterburg, N., Crittenden, S., Tesfai, M., Stolte, J., et al., 2016. Multifaceted impacts of sustainable land management in drylands: a review. Sustainability 8, 177.

McClain, M.E., 2013. Balancing water resources development and environmental sustainability in Africa: a review of recent research findings and applications. Ambio 42, 549–565.

McNamara, I., Baez-Villanueva, O.M., Zomorodian, A., Ayyad, S., Zambrano-Bigiarini, M., Zaroug, M., et al., 2021. How well do gridded precipitation and actual evapotranspiration products represent the key water balance components in the Nile Basin? J. Hydrol. Reg. Stud. 37, 100884.

Mojid, M.A., Mainuddin, M., 2021. Water-saving agricultural technologies: regional hydrology outcomes and knowledge gaps in the eastern Gangetic Plains—a review. Water 13, 636.

Mousivand, A., Arsanjani, J.J., 2019. Insights on the historical and emerging global land cover changes: the case of ESA-CCI-LC datasets. Appl. Geogr. 106, 82–92.

Mueller, B., Hirschi, M., Jimenez, C., Ciais, P., Dirmeyer, P.A., Dolman, A.J., et al., 2013. Benchmark products for land evapotranspiration: LandFlux-EVAL multi-data set synthesis. Hydrol. Earth Syst. Sci. 17, 3707–3720.

Nabil, M., Zhang, M., Wu, B., Bofana, J., Elnashar, A., 2021. Constructing a 30m African Cropland Layer for 2016 by Integrating Multiple Remote Sensing, Crowdsource, and Auxiliary Datasets. Big Earth Data.

Nhamo, L., Mabhaudhi, T., Magombeyi, M., 2016. Improving water sustainability and food security through increased crop water productivity in Malawi. Water 8, 411.

Nikiel, C.A., Eltahir, E.A.B., 2021. Past and future trends of Egypt's water consumption and its sources. Nat. Commun. 12, 4508.

Ning, S., Ishidaira, H., Wang, J., 2014. Statistical downscaling of GRACE-derived terrestrial water storage using satellite and gldas products. I_133-I_138J. Jpn. Soc Civ. Eng. 70.

Nkiaka, E., Nawaz, N.R., Lovett, J.C., 2018. Effect of single and multi-site calibration techniques on hydrological model performance, parameter estimation and predictive uncertainty: a case study in the Logone catchment, Lake Chad basin. Stoch. Env. Res. Risk A. 32, 1665–1682.

O'Connor, N., Mehta, K., 2016. Modes of greenhouse water savings. Procedia Eng. 159, 259–266.

Oki, T., Kanae, S., 2006. Global hydrological cycles and world water resources. Science 313, 1068–1072.

Osei, M.A., Amekudzi, L.K., Wemegah, D.D., Preko, K., Gyawu, E.S., Obiri-Danso, K., 2019. The impact of climate and land-use changes on the hydrological processes of owabi catchment from SWAT analysis. J. Hydrol. Reg. Stud. 25, 100620.

Ozdogan, M., Rodell, M., Beaudoing, H.K., Toll, D.L., 2010. Simulating the effects of irrigation over the United States in a land surface model based on satellite-derived agricultural data. J. Hydrometeorol. 11, 171–184.

Pan, Y., Zhang, C., Gong, H., Yeh, P.J.F., Shen, Y., Guo, Y., et al., 2017. Detection of human-induced evapotranspiration using GRACE satellite observations in the Haihe River basin of China. Geophys. Res. Lett. 44, 190–199.

Pascolini-Campbell, M., Reager, J.T., Chandanpurkar, H.A., Rodell, M., 2021. A 10 per cent increase in global land evapotranspiration from 2003 to 2019. Nature 593, 543–547.

Pedregosa, F., Varoquaux, G., Gramfort, A., Thirion, B., Michel, V., Grisel, O., et al., 2011. Scikit-learn: machine learning in python. J. Mach. Learn. Res. 12, 2825–2830.

Reinhart, V., Fonte, C.C., Hoffmann, P., Bechtel, B., Rechid, D., Boehner, J., 2021. Comparison of ESA climate change initiative land cover to CORINE land cover over Eastern Europe and the Baltic States from a regional climate modeling perspective. Int. J. Appl. Earth Obs. Geoinf. 94, 102221.

Rodell, M., Famiglietti, J.S., 1999. Detectability of variations in continental water storage from satellite observations of the time dependent gravity field. Water Resour. Res. 35, 2705–2723.

Rodell, M., Houser, P.R., Jambor, U., Gottschalck, J., Mitchell, K., Meng, C.J., et al., 2004. The global land data assimilation system. Bull. Am. Meteorol. Soc. 85, 381–394.

Schewe, J., Heinke, J., Gerten, D., Haddeland, I., Arnell, N.W., Clark, D.B., et al., 2014. Multimodel assessment of water scarcity under climate change. Proc. Natl. Acad. Sci. 111, 3245–3250.

Senay, G.B., Bohms, S., Singh, R.K., Gowda, P.H., Velpuri, N.M., Alemu, H., et al., 2013. Operational evapotranspiration mapping using remote sensing and weather datasets: a new parameterization for the SSEB approach. J. Am. Water Resour. Assoc. 49, 577–591.

Senay, G.B., Velpuri, N.M., Bohms, S., Demissie, Y., Gebremichael, M., 2014. Understanding the hydrologic sources and sinks in the Nile Basin using multisource climate and remote sensing data sets. Water Resour. Res. 50, 8625–8650.

Shen, C., 2018. A transdisciplinary review of deep learning research and its relevance for water resources scientists. Water Resour. Res. 54, 8558–8593.

Siebert, S., Burke, J., Faures, J.M., Frenken, K., Hoogeveen, J., Döll, P., et al., 2010. Groundwater use for irrigation – a global inventory. Hydrol. Earth Syst. Sci. 14, 1863–1880.

Su, F., Hong, Y., Lettenmaier, D.P., 2008. Evaluation of TRMM multisatellite precipitation analysis (TMPA) and its utility in hydrologic prediction in the La Plata Basin. J. Hydrometeorol. 9, 622–640.

Swanson, R.K., Springer, A.E., Kreamer, D.K., Tobin, B.W., Perry, D.M., 2021. Quantifying the base flow of the Colorado River: its importance in sustaining perennial flow in northern Arizona and southern Utah (USA). Hydrogeol. J. 29, 723–736.

Tabbal, D.F., Bouman, B.A.M., Bhuiyan, S.I., Sibayan, E.B., Sattar, M.A., 2002. On-farm strategies for reducing water input in irrigated rice; case studies in the Philippines. Agric. Water Manag. 56, 93–112.

Taing, L., Dang, N., Agarwal, M., Glickman, T., 2021. Water-related sustainable development goal accelerators: a rapid review. Water Security 14, 100100.

Tan, M.L., Tew, Y.L., Chun, K.P., Samat, N., Shaharudin, S.M., Mahamud, M.A., et al., 2021. Improvement of the ESA CCI Land cover maps for water balance analysis in tropical regions: a case study in the Muda River Basin, Malaysia. J. Hydrol. Reg. Stud. 36, 100837.

Tang, Q., Zhang, X., Tang, Y., 2013. Anthropogenic impacts on mass change in North China. Geophys. Res. Lett. 40, 3924–3928.

Taye, M.T., Willems, P., Block, P., 2015. Implications of climate change on hydrological extremes in the Blue Nile basin: a review. J. Hydrol. Reg. Stud. 4, 280–293.

Thornton, M.M., Shrestha, R., Wei, Y., Thornton, P.E., Kao, S., Wilson, B.E., 2020. Daymet: Daily Surface Weather Data on a 1-km Grid for North America, Version 4. ORNL Distributed Active Archive Center.

van Eekelen, M.W., Bastiaanssen, W.G.M., Jarmain, C., Jackson, B., Ferreira, F., van der Zaag, P., et al., 2015. A novel approach to estimate direct and indirect water withdrawals from satellite measurements: a case study from the incomati basin. Agric. Ecosyst. Environ. 200, 126–142.

Vinukollu, R.K., Meynadier, R., Sheffield, J., Wood, E.F., 2011. Multi-model, multi-sensor estimates of global evapotranspiration: climatology, uncertainties and trends. Hydrol. Process. 25, 3993–4010.

Wang, K., Dickinson, R.E., 2012. A review of global terrestrial evapotranspiration: observation, modeling, climatology, and climatic variability. Rev. Geophys. 50.

Wang, L., Wu, B., Elnashar, A., Zeng, H., Zhu, W., Yan, N., 2021. Synthesizing a regional territorial evapotranspiration dataset for northern China. Remote Sens. 13, 1076.

Weerasinghe, I., Bastiaanssen, W., Mul, M., Jia, L., van Griensven, A., 2020. Can we trust remote sensing evapotranspiration products over Africa? Hydrol. Earth Syst. Sci. 24, 1565–1586.

Wu, B., Zeng, H., Yan, N., Zhang, M., 2018. Approach for estimating available consumable water for human activities in a River Basin. Water Resour. Manag. 32, 2353–2368.

Xu, T., Guo, Z., Xia, Y., Ferreira, V.G., Liu, S., Wang, K., et al., 2019. Evaluation of twelve evapotranspiration products from machine learning, remote sensing and land surface models over conterminous United States. J. Hydrol. 578, 124105.

Yan, N., Tian, F., Wu, B., Zhu, W., Yu, M., 2018. Spatiotemporal analysis of actual evapotranspiration and its causes in the Hai Basin. Remote Sens. 10, 332.

Yan, J., Jia, S., Lv, A., Zhu, W., 2019. Water resources assessment of China's Transboundary River basins using a machine learning approach. Water Resour. Res. 55, 632–655.

Yoon, T., Rhodes, C., Shah, F.A., 2015. Upstream water resource management to address downstream pollution concerns: a policy framework with application to the Nakdong River basin in South Korea. Water Resour. Res. 51, 787–805.

Zeng, H., Wu, B., Zhu, W., Zhang, N., 2019. A trade-off method between environment restoration and human water consumption: a case study in ebinur Lake. J. Clean. Prod. 217, 732–741.

Zeng, H., Wu, B., Wang, S., Musakwa, W., Tian, F., Mashimbye, Z.E., et al., 2020. A synthesizing land-cover classification method based on Google Earth engine: a case study in Nzhelele and Levhuvu Catchments, South Africa. 30, 397–409.

Zhang, D., Liu, X., Zhang, Q., Liang, K., Liu, C., 2016. Investigation of factors affecting intra-annual variability of evapotranspiration and streamflow under different climate conditions. J. Hydrol. 543, 759–769.

Zhang, Y., Kong, D., Gan, R., Chiew, F.H.S., McVicar, T.R., Zhang, Q., et al., 2019. Coupled estimation of 500 m and 8-day resolution global evapotranspiration and gross primary production in 2002–2017. Remote Sens. Environ. 222, 165–182.

Zhao, W., Li, A., Deng, W., 2014. Surface energy fluxes estimation over the south Asia subcontinent through assimilating MODIS/TERRA satellite data with in situ observations and GLDAS product by SEBS model. IEEE J. Sel. Top. Appl. Earth Observ. Remote Sens. 9, 3704–3712.

Zhao, Y., Xie, Q., Lu, Y., Hu, B., 2017. Hydrologic evaluation of TRMM multisatellite precipitation analysis for Nanliu River basin in humid southwestern China. Sci. Rep. 7, 2470.

Zheng, H., Yu, G., Wang, Q., Zhu, X., He, H., Wang, Y., et al., 2016. Spatial variation in annual actual evapotranspiration of terrestrial ecosystems in China: results from eddy covariance measurements. J. Geogr. Sci. 26, 1391–1411.

Zou, M., Niu, J., Kang, S., Li, X., Lu, H., 2017. The contribution of human agricultural activities to increasing evapotranspiration is significantly greater than climate change effect over Heihe agricultural region. Sci. Rep. 7, 8805.